Dispersion and Stability Mechanism of Pt Nanoparticles on Transition-Metal Oxides

Eun-Suk Jeong
Jeonbuk National University
In-Hui Hwang
Argonne National Laboratory
Sang-Wook Han (shan@jbnu.ac.kr)
Jeonbuk National University

Article

Keywords:

Posted Date: April 13th, 2022

DOI: https://doi.org/10.21203/rs.3.rs-1543614/v1

Abstract

The heterogeneous catalysts of Pt/transition-metal oxides are typically synthesized through calcination at 500°C, and Pt nanoparticles are uniformly and highly dispersed when hydrogen peroxide (H_2O_2) is applied before calcination. The influence of H_2O_2 on the dispersion and the stability of Pt nanoparticles on titania-incorporated fumed silica (Pt/Ti-FS) supports was examined using x-ray absorption fine structure (XAFS) measurements at the Pt L_3- and Ti K-edges as well as density functional theory (DFT) calculations. The local structural and chemical properties around Pt and Ti atoms of Pt/Ti-FS with and without H_2O_2 treatment were monitored using *in-situ* XAFS during heating from room temperature to 500°C. XAFS revealed that the Pt nanoparticles of H_2O_2-Pt/Ti-FS are highly stable and that the Ti atoms of H_2O_2-Pt/Ti-FS support form into a distorted-anatase TiO_2. DFT calculations showed that Pt atoms bond more stably to oxidized-TiO_2 surfaces than they do to bare- and reduced-TiO_2 surfaces. XAFS measurements and DFT calculations clarified that the presence of extra oxygen atoms due to the H_2O_2 treatment plays a critical role in the strong bonding of Pt atoms to TiO_2 surfaces.

Introduction

Noble-metal catalysts have been widely used for various applications, including fuel cells with oxygen reduction reactions [1, 2] and hydrogen evolution reactions [3, 4]; NO_x reduction techniques such as selective catalytic reduction and lean NO_x trapping [5, 6, 7]; and photocatalysis [8]. For practical applications of noble metal catalysts, there have been many efforts to improve the dispersion and stability of noble-metal catalysts [9–11]. Many research groups have proposed different strategies through which to obtain highly-dispersed noble-metal catalysts with high catalysis efficiency and stability. For enhanced catalysis efficiency, researchers have attempted to control the morphology of nanoparticles alloyed with various metals, including Pd, Co, Ni, and Ti [12–14], and they have designed graphene-based noble-metal nanostructures [15, 16]. Heterogeneous catalysts with supports have also been extensively studied for high dispersion, because their structural and chemical properties can be modified for optimum dispersion [17–20]. For practical applications to heterogeneous catalysts, various transition-metal-oxide supports, including TiO_x, CeO_x, and ZrO_x, have been examined to enhance catalysis efficiency and selectivity [21–25]. Agglomeration of noble-metal particles on transition-metal-oxide supports is frequently observed during synthesis due to the use of a high-temperature sintering process [9–11]. Kim and co-workers showed uniformly-dispersed Pt nanoparticles with a mean diameter of less than 1 nm on transition-metal-oxide supports [9, 10, 26]. They argued that the agglomeration of noble-metal particles on transition-metal-oxide supports could be avoided using a hydrogen peroxide (H_2O_2) treatment. However, the dispersion and stability mechanism of noble metal on transition-metal-oxide supports with an H_2O_2 treatment during the synthesis process remains unclear and needs to be elucidated.

H_2O_2 treatments have been widely used in various fields, including organic and inorganic chemical sciences, material science, and biological science. Previous studies have shown that H_2O_2 treatments could alter the oxidation states and local structural properties around transition-metal atoms [27–34]. Researchers have reported that H_2O_2 treatments cause a red shift of the ZnO bandgap and enhance the crystal quality of ZnO nanorods [31, 32]. With H_2O_2 treatments, the improved morphology of ZrO_2 particles [35], the crystal structure and the exposed surface changes of TiO_2 [31], and the aggregation of amorphous calcium phosphate nanoparticles [34] were observed as well. Previous studies strongly suggested that H_2O_2 treatments significantly affect both the outermost surfaces and internal structures of materials without matter of the crystallization. Microscopic measurements are needed to understand the influence of H_2O_2 on the surfaces, interfaces, and internal structures of the materials. Heterogeneous Pt/TiO_2 catalysts are widely used for practical applications. Pt nanoparticles are highly dispersive and quite stable on TiO_2 supports when H_2O_2 treatment is used. In this study, we examined the effects of H_2O_2 on the bonds of Pt nanoparticles to TiO_2 supports to understand the dispersion and stability of noble-metal catalysts on transition-metal-oxide supports.

The influence of H_2O_2 on the stoichiometric change, morphology, and crystal structure of metal nanoparticles has been examined using scanning electron microscopy (SEM), transmission electron microscopy (TEM), and X-ray diffraction (XRD) measurements [27, 31, 34]. However, SEM, TEM, and XRD measurements are limited in their quantitative characterizations of the effects of H_2O_2 treatment on the dispersion of and local structural change in metal nanoparticles during the synthesis process, because most nanoparticles are amorphous and in the sub-nanometer scale in size. X-ray absorption fine structure (XAFS) is a suitable tool for investigating the local structural and chemical properties around a selected species atom of compounds. XAFS is particularly useful for in-situ examinations of the local structural and chemical property changes of heterogeneous compounds on the nanometer scale [18, 11, 36]. The local structural and chemical properties around the noble-metal and transition-metal atoms of noble metal/transition-metal-oxide catalysts were examined using *in-situ* XAFS measurements at the absorption edges of the noble-metal and the transition-metal atoms. As a complement to the XAFS measurements, density functional theory (DFT) calculations were performed to elucidate the stability of the bonds between noble metal and metal-oxide support. We observed that the presence of extra oxygen atoms due to the H_2O_2 treatment plays an important role in the high dispersion and stability of Pt nanoparticles on TiO_2 supports.

Results

Temperature-dependent XANES spectra. For this study, Pt nanoparticles were synthesized on titania-incorporated fumed silica (Ti-FS) supports with and without H_2O_2 treatment [9,10], as summarized in Fig. 1. The size and the distribution of Pt nanoparticles were examined by energy dispersive spectroscopy (EDS) and TEM measurements, as shown in Fig. 2. X-ray absorption near edge structure (XANES) is sensitive to the chemical valence state as well as the geometry of the nearest neighboring atoms around a probing atom [37,38]. Temperature-dependent XANES at the Pt L_3 edge shows a dramatic change in the white line intensity during heating, as shown in Figs. 3 (a) and (b). Changes in the Pt white line are known to be directly related to Pt oxidation

[11,39,40]. Jeong *et al.* clarified that the white line area of Pt L_3 edge directly corresponds to the coordination number of oxygen atoms bonding to Pt atoms [11]. When a Pt atom bonds with oxygen atoms, the empty state density of the Pt 5d orbitals increases because the electrons in the Pt 5d orbitals transfer to the oxygen atoms. The strong intensity of the white line and the slight shift toward a higher energy of the Pt absorption edge of both Pt/Ti-FS and H_2O_2-Pt/Ti-FS at the RT indicate a high oxidation of Pt atoms compared to those of a Pt foil, as shown in Figs. 3 (a) and (b). The white line features strongly suggest that the Pt atoms on Ti-FS supports with no matter of the H_2O_2 treatment at RT are oxidized with PtO_x. The intensity of the Pt white line of H_2O_2-Pt/Ti-FS at the RT is considerably stronger than that of Pt/Ti-FS at RT, as shown in Figs. 3 (a) and (b), respectively. This indicates that the mean oxidation state of Pt atoms of H_2O_2-Pt/Ti-FS is higher than that of Pt atoms of Pt/Ti-FS, which is attributed to the H_2O_2 treatment. When heated up to 250°C, the intensities of the white lines of both Pt/Ti-FS and H_2O_2-Pt/Ti-FS decrease dramatically, and the absorption edges shift toward a lower energy, which is the nearly same as the absorption edge of a Pt foil at RT. The temperature-dependent behavior of the white line strongly implies that the Pt atoms of both Pt/Ti-FS and H_2O_2-Pt/Ti-FS are rapidly reduced in an H_2 environment during heating, and that most of the oxygen atoms dissociate from the Pt nanoparticles at 250°C.

The chemical valence state and the local structural properties around the Ti atoms of Pt/Ti-FS and H_2O_2-Pt/Ti-FS supports are also changed with those around the Pt atoms during the synthesis and heating processes. A change around the Ti atoms of Ti-FS supports is crucial for understanding the dispersion mechanism of Pt nanoparticles on the supports. Figures 3 (c) A – C show XANES spectra of Ti-FS supports at the Ti K edge during the temperature change of RT → 500°C → RT^c in an H_2 environment. The XANES spectra of the Ti-FS supports at RT and RT^c are nearly identical, implying a lack of changes in the local structural and chemical properties around the Ti atoms of Ti-FS supports for the calcining process. The XANES of H_2O_2-Ti-FS reveals that H_2O_2 treatment significantly affects the local structural and chemical properties around the Ti atoms of Ti-FS, as shown in Fig. 3 (c) D. The increased intensity of the white line in Fig. 3 (c) D indicates that an H_2O_2 treatment affects the oxidation of the Ti atoms of the supports. To elucidate the dispersion mechanism of Pt nanoparticles on Ti-FS supports, it is important to have a direct comparison of the XANES spectra of Pt/Ti-FS with and without H_2O_2 treatment at the Ti K edge as well as at the Pt L_3 edge. Figures 3 (c) E–G and H–J, respectively, show the XANES spectra of Pt/Ti-FS without and with H_2O_2 treatment at the Ti K edge. The XANES spectra of Pt/Ti-FS and H_2O_2-Pt/Ti-FS are nearly identical to each other while being substantially different from those of Ti-FS and H_2O_2-Ti-FS, as shown in Figs. 3 (c) A–J. This finding strongly suggests that the local structural and chemical properties around the Ti atoms of Ti-FS supports are significantly affected by a Pt impregnating process during the synthesis of Pt/Ti-FS. The XANES spectra show that the local structure around the Ti atoms of Pt/Ti-FS and H_2O_2-Pt/Ti-FS is close to an anatase TiO_2. Pt atoms might serve as a catalyst to the Ti atoms, as a TiO_2 was formed when tetra amine platinum nitrate was applied to Ti-FS during the synthesis. The structural properties around the probing Pt and Ti atoms of Pt/Ti-FS systems at the Pt L_3 and Ti K edges, respectively, can be more clearly seen in more detail in extended XAFS (EXAFS), which shows small oscillations above the absorption edges.

Temperature-dependent local structural properties. EXAFS can be used to quantitatively determine the local structural properties around a selected species atom of compounds [41-43]. After atomic background function was determined using the AUTOBK code [44], EXAFS data was extracted from XAFS and Fourier transformed to the r-space, as shown in Fig. 4. EXAFS was quantitatively analyzed with the IFEFFIT package [45] using standard analysis procedures [43,46]. The peak positions of EXAFS data correspond to the atomic shell distances from a probing atom. The peak positions of the EXAFS data are approximately 0.3 Å shorter than the true distances of atomic pairs because the phase shift of back-scattered photoelectrons by neighboring atoms has not yet to be considered. The temperature-dependent EXAFS of Pt/Ti-FS with and without H_2O_2 treatment reveals that the local structure around Pt atoms is significantly changed by heating, as shown in Figs. 4 (a) and (b). At RT the first and second peaks of ~1.7 Å and 2.2 Å respectively correspond to O and Pt atoms [11]. The first peak intensity gradually weakens during heating, and it virtually disappears at 250°C. This indicates that Pt atoms initially bond with oxygen atoms as well as Pt atoms, and that there is a lack of Pt-O bonds at high temperatures. After being heated up to 500°C and cooled down to RT (RT^c), the local structures around the Pt atoms of both Pt/Ti-FS and H_2O_2 Pt/Ti-FS at RT^c are nearly identical to those above 250°C, strongly implying that Pt nanoparticles have a stable structure due to the calcining process. This result is consistent with the XANES measurements of Pt/Ti-FS and H_2O_2 Pt/Ti-FS. EXAFSs at the Pt L_3 edge of both Pt/Ti-FS and H_2O_2 Pt/Ti-FS show prominent peaks at approximately 2.2 Å and 2.8 Å when heated above 200°C; these peaks are expected to be Pt-Pt pairs. Above 200°C, the lack of any change in the temperature-dependent EXAFS of Pt-Pt pairs strongly implies a stable structure of Pt atoms in particular in H_2O_2-Pt/Ti-FS. EXAFS measurements of H_2O_2-Pt/Ti-FS at the Pt L_3 edge reveal that oxygen atoms wrapping the tops of Pt nanoparticles are mostly dissociated, while Pt atoms form into stable Pt nanoparticles, tightly bonded to the Ti-FS supports, when heated up to 250°C.

EXAFS of Ti-FS at the Ti K-edge shows the first and second peaks at 1.7 Å and 2.5 Å, respectively, as shown in Figs. 4 (c) A and C. These peaks respectively correspond to the Ti-O and Ti-Ti pairs of a TiO_2 structure [46,47]. The distance of the Ti-Ti pairs is expanded due to the H_2O_2 treatment, as shown in Fig. 4 (c) D. The EXAFS of Ti-FS at the Ti K edge indicates that the TiO_2 of the Ti-FS has a quite unstable structure, because the peak positions and shapes of EXAFS substantially depend on the H_2O_2 treatment. The local structure around the Ti atoms of Pt/Ti-FS is considerably different from that before the Pt precursor is impregnated on Ti-FS, as shown in Fig. 4 (c). EXAFS of H_2O_2-Pt/Ti-FS shown in Figs. 4 (c) H–J clearly shows three peaks at ~1.5 Å, ~2.3 Å, and ~3.2 Å. The local structure around the Ti atoms of Pt/Ti-FS is substantially different from that of H_2O_2-Pt/Ti-FS, particularly at 250°C, as shown in Figs. 4 (c) G and J. The EXAFS peak positions of H_2O_2-Pt/Ti-FS at the Ti K edge show a lack of changes, whereas they exhibit some changes in Pt/Ti-FS during heating from RT to 250°C. This finding strongly suggests that the local structure around the Ti atoms of H_2O_2-Pt/Ti-FS is quite stable and analogous to an anatase TiO_2. The quantitative local structural properties can be obtained by fitting the EXAFS data to the EXAFS theoretical calculations using a structural model [49].

Quantitative analysis of local structural properties. Using the standard fitting procedures, EXAFS data in the r-space were fitted to EXAFS theoretical calculations with different structural models at the Pt L_3 and Ti K edges [43,46]. The structural models of EXAFS theoretical calculations were designed based on the measured XANES and EXAFS data. PtO_x and Pt foil structures were initially modeled for the low and high temperatures of both Pt/Ti-FS and H_2O_2-Pt/Ti-FS, respectively. At intermediate temperatures, a mixture structure of PtO_x and Pt foil was used to fit EXAFS data. For the EXAFS data fitting of the Ti K edge, structural models were selected based on the XANES and EXAFS data of Ti-FS and Pt/Ti-FS. In the fitting of the EXAFS data of H_2O_2-Pt/Ti-FS, a distorted-anatase TiO_2 structure was used for the EXAFS theoretical calculations. EXAFS theoretical calculations were done using the FEFF8 code [49], and EXAFS data was fitted using the IFEFFIT package [45]. In the fittings, the distance, the coordination number, and the Debye-Waller factors (, including thermal vibration and static disorder) of each atomic shell were varied. Only single-scattered paths were included in the fittings; this decision was made because, due to the particle size and the structural disorder, the EXAFS signal of a multiple-scattered path of nanoparticles is much weaker than that of a single-scattered path. A k-weight fit was used to reduce the correlation between and coordination number [50].

Figure 5 shows representative EXAFS data and the best fits. The quantitative structural properties around the Pt and Ti atoms of Pt/Ti-FS and H_2O_2-Pt/Ti-FS were obtained from the goodness fits of the EXAFS data. The results of the best fits are summarized in Tables 1–3. EXAFS at the Pt L_3 edge reveals that a Pt atom of Pt/Ti-FS and H_2O_2-Pt/Ti-FS initially bonds with approximately five and six oxygen atoms, respectively. Pt atoms of Pt/Ti-FS initially have the second and third neighbors of ten Pt atoms at the respective distances of ~2.8 Å and ~3.1 Å. This indicates that Pt atoms are partially oxidized and have Pt-Pt bonds at RT. When heated above 250°C, the Pt atoms of both Pt/Ti-FS and H_2O_2-Pt/Ti-FS form into Pt nanoparticles with a substantial amount of structural disorder, compared to that of the Pt foil. When H_2O_2 treatment is applied on Pt/Ti-FS at RT, Pt atoms have the first and second neighbors of six O and eight Pt atoms at the respective distances of ~2.0 Å and ~3.28 Å. Due to the H_2O_2 treatment, the distance of Pt-Pt pairs is elongated and the coordination number of oxygen atoms around Pt atoms is increased, compared to those of Pt/Ti-FS. This finding indicates that, due to the H_2O_2 treatment, oxygen atoms penetrate into Pt nanostructures, thus cracking Pt-Pt bonds at RT. The O atoms between Pt atoms play a decisive role in a high dispersion of Pt nanoparticles; meanwhile, their existence at the interface of Pt nanoparticles and Ti-FS supports assists a strong bond between Pt atoms and TiO_2 supports at high temperatures. When heated above 250°C, the coordination number of Pt atoms of Pt/Ti-FS is gradually increased to be ~10 at 500°C, whereas that of H_2O_2-Pt/Ti-FS shows a lack of changes in the temperature range of 250 – 500°C. This result strongly implies that, at high temperatures, the Pt atoms of Pt/Ti-FS and H_2O_2-Pt/Ti-FS move to become lumpy and are pinned on the supports, respectively. A large σ^2 value of the Pt-Pt pairs of Pt/Ti-FS indicates a less stable structure of Pt nanoparticles than that of H_2O_2-Pt/Ti-FS, particularly at RT[c]. When cooled down to RT from 500°C, the local structural properties around Pt atoms of both Pt/Ti-FS and H_2O_2-Pt/Ti-FS are nearly the same as those at 500°C, except for the σ^2 values of Pt-Pt pairs due to the thermal effect. Jeong and co-workers demonstrated using EXAFS measurements that the Pt nanoparticles of H_2O_2-Pt/Ti-FS likely have a pancake shape on TiO_2 supports [11]. In this case, Pt nanoparticles stably bond to the supports with a high catalysis efficiency. At RT[c], the bond lengths of the Pt-Pt pairs of both Pt/Ti-FS and H_2O_2-Pt/Ti-FS are shorter than that of a Pt foil due to the effects of nanoparticle boundaries with dangling bonds [50].

The EXAFS data of Ti-FS and Pt/Ti-FS with and without H_2O_2 treatment at the Ti K edge were also analyzed in the same manner as the EXAFS data analysis at the Pt L_3 edge, and the best fit results are summarized in Table 3. The best fit of EXAFS data at the Ti K edge suggests that the Ti atoms of Ti-FS form Ti-O complexes in the temperature range of RT – 250°C. When an H_2O_2 treatment is applied on Ti-FS, the local structures around Ti atoms are substantially changed; however, they do not form into a crystalline structure. The EXAFS data of Pt/Ti-FS and H_2O_2-Pt/Ti-FS at the Ti K edge shows the Ti-O(1), Ti-O(2), Ti-Ti(1), and Ti-Ti(2) pairs. This means that the Ti atoms of Pt/Ti-FS and H_2O_2-Pt/Ti-FS form a TiO_2 crystalline structure, although there is still a substantial amount of structural distortion in the atomic pairs. In an anatase TiO_2, a Ti atom consists of a Ti-O octahedron with six O atoms. The slightly low coordination of O atoms of Pt/Ti-FS and H_2O_2-Pt/Ti-FS indicates the existence of some vacancies on the O sites of the octahedrons. The coordination numbers of both the O and Ti atoms of the Pt/Ti-FS and H_2O_2-Pt/Ti-FS remain constant during heating. For the Pt/Ti-FS, the low coordination of Ti atoms and the large σ^2 value of Ti-Ti pairs, particularly at 250°C, indicate an incomplete TiO_2. It is worth noting that σ^2 values can be gradually increased at temperatures above 100 K due to the thermal vibration of atomic pairs [37,46]. Compared to that at RT, the σ^2 value of the Ti-Ti pairs of H_2O_2-Pt/Ti-FS decreased when heated up to 250°C. This finding strongly suggests that the TiO_2 particles of H_2O_2-Pt/Ti-FS form into a more stable crystalline structure at 250°C. The distance change of the Ti-O and Ti-Ti pairs of H_2O_2-Pt/Ti-FS serves as further evidence of TiO_2 crystallization at 250°C, compared to that at RT. The EXAFS measurements at the Ti K edge reveal that the Ti atoms form a distorted-anatase TiO_2 in H_2O_2-Pt/Ti-FS, whereas the Ti atoms do not form a stable crystalline structure in Pt/Ti-FS. The in-situ EXAFS measurements indicate that the Pt precursor and the H_2O_2 treatment in succession assist the Ti atoms of Ti-FS in forming into a crystalline structure.

Discussion

DFT calculations of Pt atoms on TiO_2 surfaces. The interfacial structures of Pt atoms and TiO_2 supports certainly affect the dispersion and the stability of Pt nanoparticles. Based on the EXAFS measurements, DFT calculations were performed using the CASTEP code in the Materials Studio to understand the bonds between the Pt atoms and TiO_2 supports at the interfaces [52]. For the DFT calculations, the TiO_2(101) surface is chosen because its surface has better thermodynamic stability than the other surfaces [53-55]. A 2×3 supercell slab with twenty-four TiO_2 molecular units, which includes four Ti layers and eight O layers, is used in this study to construct the anatase TiO_2(101) surface that is similar to those used in previous studies [56-58]. It has dimensions of 11.4 Å × 11.4 Å × 20 Å containing a vacuum region of about 15 Å to avoid interactions between the periodically-repeated slabs and to separate the slabs. Figures 6 (a) and (b) show a part of the TiO_2(101) surface of the supercell slab. In the calculations, the atoms of the bottom two layers

—i.e., the lower half of the slab—are fixed at the original positions of anatase TiO_2, and the rest of the atoms are allowed to freely move their positions to minimize the total energy of the system. A Pt atom is added on three different TiO_2(101) surfaces, such as bare-TiO_2, oxidized-TiO_2, and reduced-TiO_2, as shown in Fig. 6 (c), (d), (e), respectively. Oxidized- and reduced-TiO_2(101) surfaces are generated by adding one O atom on the top of the 5cTi atom and by removing the bridging O atom (2cO), respectively, as shown in Figs. 6 (d) and (e), respectively [59]. Pt adatoms are initially placed in the middle of the hexagons of the TiO_2(101) surfaces in Figs. 6 (c_1), (d_1), and (e_1). After DFT calculations, the final locations of the Pt atoms are shown in Figs. 6 (c_2)-(c_3), (d_2)-(d_3), and (e_2)-(e_3).

Before the DFT calculations, we first examined the cutoff energy of plane waves in the range of 300 – 700 eV and the k-point grid using the Monkhorst-Pack method to reduce the computation time and obtain sufficient precision. The ultra-soft pseudopotentials with a cutoff energy of 550 eV, 3×3×2 k-point grids, and Perdew-Burke-Ernzerhof (PBE) functional of the generalized gradient approximation (GGA) are used [60]. The top layers of the slab including Pt adatoms and overlayers are relaxed until the force is less than 0.1 eVÅ^{-1} in the Cartesian coordinates. The calculation is terminated when the total energy difference between the present and final calculations converges to less than 5×10^{-5} eV per atom. The binding energy of a Pt atom on TiO_2 is defined as $\triangle E = E_{Pt/TiO2} - E_{TiO2} - E_{Pt}$, where $E_{Pt/TiO2}$ is the total energy of a Pt atom on TiO_2; E_{TiO2} is the total energy of a TiO_2 slab for bare-TiO_2, oxidized-TiO_2, and reduced-TiO_2 cases; and E_{Pt} is the total energy of a single Pt atom. The DFT calculations show $\triangle E$ = -2.145 eV, -6.515 eV, and -4.455 eV for bare TiO_2, oxidized TiO_2, and reduced TiO_2, respectively. This result indicates that Pt atoms more strongly bond to oxidized or reduced TiO_2 than they do to bare TiO_2. A strong bond of Pt atoms to reduced-TiO_2 surface corresponds to a strong metal-support interaction (SMSI). Previous studies have shown that the catalysis efficiency of noble-metal on transition-metal-oxide supports decreases by reduction at a high temperature due to an SMSI [61-63]. The DFT calculations show that the bond of Pt atoms to oxidized TiO_2 is more stable than the bond of Pt atoms to the others, as shown in Fig. 6. In this study, we first report a strong bond of Pt atoms to oxidize-TiO_2 surfaces, which is the origin of the high dispersion and high stability of Pt atoms on Ti-FS supports, based on the EXAFS measurements and the DFT calculations.

Wavelet-transformed EXAFS analysis. The DFT calculations suggest that there are Pt-O bonds at the interfaces of Pt/TiO_2 during the processes of the H_2O_2 treatment and the heating above 250^{o}C. Since Fourier-transformed (FT) EXAFS analysis does not show a distinguishable feature of Pt-O pairs, as shown in Fig. 5, we performed the wavelet-transformed (WT) EXAFS analysis which has structural information in the k-space as well as in the r-space. Figure 7 shows the WT-EXAFS images of the Pt foil and the H_2O_2-Pt/Ti-FS at different temperatures. The EXAFS signal of the Pt atoms of the Pt foil in the k- and r-spaces is quite different from that of the O atoms around a probing Pt atom of the H_2O_2-Pt/Ti-FS, as shown in Figs. 7 (a) and (b), respectively. The signals of WT-EXAFS near 1.5 Å and 2.5 Å correspond to the nearest O and Pt atoms around the probing a Pt atom, respectively. The WT-EXAFS signals of the O and Pt atoms are horizontally distributed around the peaks at ~6.5 Å^{-1} and ~9.5 Å^{-1}, respectively. Figure 7 (b) shows that the O signal of the H_2O_2-Pt/Ti-FS is dominant over the Pt signal at the RT. When the H_2O_2-Pt/Ti-FS is heated up to 200^{o}C, the O signal decreases and the Pt signal clearly appears. This agrees well with the FT-EXAFS results, as shown in Table 2. Figure 7 (d) shows a weak but definite signal of O atoms. This indicates the presence of Pt-O pairs of H_2O_2-Pt/Ti-FS at RT^c. After the reduction process of heating up to 500^{o}C in an H_2 environment, the absence of oxygen atoms is expected at the surfaces of Pt nanoparticles. The WT-EXAFS signal of Pt-O pairs at RT^c likely indicates Pt-O bonds at the interface of Pt/TiO_2. This corresponds to the DFT calculations. Since the EXAFS signal of Pt-O pair of H_2O_2-Pt/Ti-FS at RT^c is considerably weak, it may not be fully detected by the Fourier transformed EXAFS due to the resolution limit.

The mean diameters of the Pt nanoparticles of H_2O_2-Pt/Ti-FS and Pt/Ti-FS are estimated to be ~11 Å and ~22 Å for the Pt coordination numbers of 7.9 and 9.6, respectively, using a hemispherical model [11]. The mean diameters suggest that an H_2O_2 treatment prevents the agglomeration of Pt atoms on TiO_2 at high temperatures. The SMSI effects of noble metal/transition-metal oxides have been observed on several different systems [61-63]. Heterogeneous catalysts of noble-metal nanoparticles/transition-metal-oxide supports are widely used for practical applications [21-24]. With an H_2O_2 treatment, oxygen atoms penetrate into Pt/Ti-FS and form the bond of Pt-O-Ti at the interface of Pt/TiO_2, as shown in Figs. 6 (d_2) and (d_3). The interfaces of Pt atoms and TiO_2 supports are initially somewhat unstable due to dangling bonds of the TiO_2 surface. When H_2O_2 is applied to Pt/TiO_2, an additional oxygen atom forms a stable Pt-O-Ti bond at the interface, thus reducing the surface energy. The additional oxygen atoms at the interface simultaneously bond with Pt and Ti atoms, and they form a Ti-O octahedron. As a result, the Pt atoms on Ti-FS supports are restricted and do not aggregate at high temperatures. A lack of change of the Pt coordination numbers of H_2O_2-Pt/Ti-FS in the temperature range of 200 – 500^{o}C and at RT^c, as shown in Table 2, indicates that the bonds of Pt atoms to TiO_2 surfaces are considerably strong and remain constant even at 500^{o}C. This finding is consistent with the conversion results of the heterogeneous catalysts of H_2O_2-Pt/Ti-FS [65].

Oxidation due to H_2O_2 treatments has been observed in many different transition-metal systems, including Co, Zr, Mn, Ti, Zn, and Cr [27-30,32,33,35]. Imamura and co-workers suggested that H_2O_2 molecules on a metal surface are converted into hydroxyl anions and hydroxyl radicals (*OH) as follows [66], $H_2O_2 + e^- \rightarrow {}^*OH + [OH]^-$. Previous studies have shown that an H_2O_2 treatment changes the surface morphology of metals, assists the bonds of heterogeneous metal atoms, and causes oxidation of metal surfaces [27-30,32,33,35]. Our XAFS measurements and DFT calculations are consistent with the previous reports. When the Pt precursors are embedded into Ti-FS supports during the synthesis of Pt/Ti-FS catalysts, they randomly bond to the surfaces of TiO_x complexes. Our XAFS measurements indicate that the Pt precursors serve as catalysts, thereby inducing TiO_x to a rough TiO_2 structure which is more stable than TiO_x. Applying H_2O_2 to Pt/Ti-FS oxidizes both Pt and Ti atoms, and the additional oxygen atoms bond with Pt and Ti atoms at the interface of Pt/TiO_2. This scenario is consistent with the changes in the coordination numbers of O atoms around the Pt and Ti atoms at RT, as listed in Tables 1 – 3. An H_2O_2 treatment further induces a stable structure TiO_2. When H_2O_2-Pt/Ti-FS is heated in an H_2 environment, the O atoms gradually

dissociate from the Pt atoms, and the deoxidized Pt atoms form into stable Pt nanoparticles with a uniform size on the TiO_2 supports, which change to a more stable crystal at high temperatures. The additional O atoms stemming from the H_2O_2 treatment tightly grasp Pt atoms on TiO_2 supports. This finding is consistent with the EXAFS measurements that show a lack of change of local structures of Pt nanoparticles at RT^c, compared to those at 500^{o}C. Our results correspond to inactive and stable transition-metal oxides with the extra O atoms which exist at the outermost boundaries [67-69]. When the H_2O_2 treatment was performed to Ti-FS supports before Pt nanoparticles were embedded (data not shown here), the dispersion and stability of Pt/TiO_2 were nearly the same as the results shown here. This indicates that the dispersion and stability of Pt/TiO_2 are independent of the order of an H_2O_2 treatment before and after Pt nanoparticles are embedded on Ti-FS supports.

Conclusion

XAFS measurements and DFT calculations show that the additional oxygen atoms at the interface of Pt/TiO_2 play an important role in the dispersion and stability of Pt nanoparticles. The additional oxygen atoms can be simply supplied by an H_2O_2 treatment. XAFS measurements at the Pt L_3 and Ti K edges reveal that, when H_2O_2-Pt/Ti-FS is heated above 250^{o}C in an H_2 environment, Pt atoms form into stable nanoparticles with a high dispersion on TiO_2 supports. The heterogeneous catalysts of Pt/TiO_2 with H_2O_2 treatment are considerably stable without Pt aggregation in the temperature of RT – 500^{o}C. DFT calculations suggest that a strong bond of Pt-O-Ti is formed at the interface of Pt/TiO_2. WT-EXAFS confirmed the presence of the Pt-O pairs which exist at the interface of Pt/TiO_2. The results of this study show that H_2O_2 treatment is a new strategy for the synthesis of various heterogeneous catalysts of noble-metal/transition-metal-oxide systems with high dispersion. The stability issue of heterogeneous catalysts for practical applications can also be resolved using an H_2O_2 treatment.

Methods

Synthesis of Pt nanoparticles/Ti-FS supports. Fumed silica (FS) which was commercially obtained from Sigma-Aldrich was dehydrated with anhydrous ethanol with a purity of 99.9% and subsequently reacted with titanium butoxide (Sigma-Aldrich) with the purity of 99% dissolved in ethanol. Titania-incorporated fumed silica (Ti-FS) was obtained by washing with ethanol and subsequently drying at 80°C. After Ti-FS was calcined at 500°C for two hours, it was impregnated with tetra amine platinum nitrate with a purity of 99%, which was purchased from Sigma-Aldrich, using an incipient wetness method. The amount of Pt was approximately 4 *wt*% of the silica weight. The catalysts of Pt on Ti-FS supports (Pt/Ti-FS) were dried at 80°C. After H_2O_2 treatments were applied to both calcined Ti-FS and Pt/Ti-FS, H_2O_2-Ti-FS and H_2O_2-Pt/Ti-FS were dried at 80°C. The synthesis procedures of the catalysts of Pt/transition-metal-oxide supports have previously been described in detail elsewhere [9,10]. For in-situ XAFS measurements, we prepared Pt/Ti-FS, H_2O_2-Pt/Ti-FS, Ti-FS, and H_2O_2-Ti-FS. The synthesis procedure of the specimens and the conditions of XAFS measurements are summarized in Fig. 1.

EDS and TEM measurements. EDS measurements were performed to analyze the distribution of selected species atoms of the H_2O_2-Pt/Ti-FS specimen, as shown in Fig. 2. The EDS images show that Pt atoms are uniformly distributed over the entire sample. TEM images indicate that the size of Pt particles on FS is approximately 10 nm, meanwhile it is ~2 nm for the Pt/Ti-FS and H_2O_2-Pt/TI-FS specimens. The size of Pt nanoparticles becomes more uniform when H_2O_2 treated on Pt/Ti-FS. This agrees well with previous reports [9,10].

***In-situ* XAFS measurements.** In-situ XAFS measurements were taken of Pt/Ti-FS specimens with and without H_2O_2 treatment at the Pt L_3 edge (11,564 eV) and the Ti K edge (4,965 eV) with a transmission mode under H_2 environment in the temperature range of room temperature (RT) – 500°C. The XAFS measurements were carried out by selecting the incident x-ray energy with a three-quarters-tuned Si(111) double crystal monochromator at the 9BM beamline of the Advanced Photon Source (APS) and at the 8C beamline of the Pohang Light Source II (PLS II). To avoid self-absorption effects, the specimen powders were ground and sieved with a sieve having a mean size of 25 μm. The powders were homogeneously mixed with a boron-nitrite powder and pressed into a disk shape with a proper thickness in a hole of a copper sample holder for the absorption edge step sizes of 0.3 – 0.8 at both the Pt L_3 and Ti K edges [37]. The specimens were maintained at a constant and uniform temperature during the XAFS scans.

Declarations

Acknowledgment

The authors would like to thank Dr. M.-Y Kim for her technical assistance on the synthesis of Pt/Ti-FS and H_2O_2-Pt/Ti-FS specimens. The work was conducted under the auspices of the Basic Science Research Program through the National Research Foundation of Korea government grant funded by the Ministry of Education (No. 2020K1A3A7A09080403, No. 2021R111A3047300). XAFS data were collected at the 9BM beamline of APS in USA and the 8C beamline of PLS II in Korea. This research used resources of APS, an Office of Science User Facility operated for the U.S. Department of Energy (DOE) Office of Science by Argonne National Laboratory, and was supported by the U.S. DOE under Contract No. DE-AC02-06CH11357, and the Canadian Light Source and its funding partners.

Author contributions

E.-S.J., I.-H.H., and S.-W.H. performed XAFS measurements. E.-S.J. prepared the specimens, XAFS data analysis, and DFT calculations. S.-W.H. designed this study and wrote the paper. All authors reviewed the manuscript.

References

1. Z. Tang, W. Wu, K. Wang, Catalysts 8 (2018) 65.
2. J. W. Lee, B. N. Popov, J. Solid State Electrochem. 11 (2007) 1355.
3. C. Li. J. B. Baek, ACS Omega 5 (2020) 31.
4. N. Cheng. S. Stambula, D. Wang, M. N. Banis, J. Liu, A. Riese, B. Xiao, R. Li, T.-K. Sham, L.-M. Liu, G. A. Botton, X. Sun, Nat. Commun, 7 (2016) 13638.
5. C. Yin, L. Wang, S. Rivillon, A. J. Shih, R. T. Yang, Catal. Lett. 145 (2015) 1491.
6. Z. Zhang, M. Chen, W. Shangguan, Catal. Commun, 10 (2009) 1330.
7. M. Mihet, M. D. Lazar, V. Almasan, V. Mirel, AIP Conf. Proc. 1425 (2012) 73-76.
8. J.-H. Lee, H.-J. Ahn, J.-I. Youn, Y.-J. Kim, S.-J. Suh, H.-J. Oh, Korean J. Met. Mater. 57 (2019) 510.
9. M.-Y. Kim, S. M. Park, J.-H. Park, C. H. Shin, W. J. Moon, N. E. Sung, G. Seo, Reac. Kinet. Mech. Cat. 103 (2011) 463.
10. M.-Y. Kim, Y. S. You, H.-S. Han, G. Seo, Catal. Lett. 120 (2008) 40.
11. E.-S. Jeong, C.-I. Park, Z. Jin, I.-H. Hwang, J.-K. Son, M.-Y. Kim, J.-S. Choi, S.-W. Han, Catal. Lett. 145 (2015) 971.
12. U. A. Paulus, A. Wokaun, G. G. Scherer, T. J. Schmidt, V. Stamenkovic, V. Radmilovic, N. M. Markovic, P. N. Ross, J. Phys. Chem. B 106 (2002) 4181.
13. C. Gümeci, Z. Li, D. J. Casadonte Jr., C. Korzeniewski, J. Electrochem. Soc. 159 (2012) F35.
14. L. Zhang, K. Lee, J. Zhang, Electrochim. Acta. 52 (2007) 3088.
15. M. Giovanni, H. L. Poh, A. Ambrosi, G. Zhao, Z. Sofer, F. Saněk, B. Khezri, R. D. Webster, M. Pumera, Nanoscale 4 (2012) 5002.
16. C. Tan, X. Huang, H. Zhang, Mater. Today 16 (2013) 29.
17. L. Liu, A. Corma, Chem. Rev. 118 (2018) 4981.
18. K. Asakura, Y. Iwasawa, H. Kuroda, J. Chem. Soc., Faraday Trans. 1 (1988) 1329.
19. T. W. V. Deelen, C. H. Mejia, K. P. de Jong, Nat. Catal. 2 (2019) 955.
20. H. Tang, Y. Su, B. Zhang, A. F. Lee, M. A. Isaac, K. Wilson, L. Li, Y. Ren, J. Huang, M. Haruta, B. Qiao, X. Liu, C. Jin, D. Su, J. Wang, T. Zhang, Sci. Adv. 3 (2017) e1700231.
21. M. Macino, A. J. Barnes, S. M. Althahban, R. Qu, E. K. Gibson, D. J Morgan, S. J. Freakley, N. Dimitratos, C. J. Kiely, X. Gao, A. M. Beale, D. Bethell, Q. He, M. Sankar, G. J. Hutchings, Nat. Catal. 2 (2019) 873.
22. C.-J. Pan, M.-C. Tsai, W.-N. Su, J. Rick, N. G. Akalework, A. K. Agegnehu, S.-Y. Cheng, B.-J. Hwang, J. Taiwan Inst. Chem. Eng. 74 (2017) 154.
23. A. Bruix, A. Migani, G. N. Vayssilov, K. M. Neyman, J. Libuda, F. Illas, Phys. Chem. Chem. Phys. 13 (2011) 11384.
24. Y. Nagai, K. Dohmae, K. Teramura, T. Tanaka, G. Guilera, K. Kato, M. Nomura, H. Shinjoh, S. Matsumoto, Catal. Today 145 (2009) 279.
25. Andrew (Bean) Getsoian, Joseph R. Theis, William A. Paxton, Michael J. Lance, and Christine K. Lambert, Nat. Cat. 2 (2019) 614.
26. M.-Y. Kim, G. Seo, J.-H. Park, C.-H. Shin, E. S. Kim, Korean Chem. Eng. Res. 49 (2011) 1.
27. Y. Gultneh, T. B. Yisgedu, Y. T. Tesema, R. J. Butcher, Inorg. Chem. 42 (2003) 1857.
28. H. Kitagishi, M. Tamaki, T. Ueda, S. Hirota, T. Ohta, Y. Naruta, K. Kano, J. Am. Chem. Soc. 132 (2010) 16730.
29. Q.-E. Cao, Y. Zhao, S. Wu, Z. Hu, Q. Xu, Talanta 51 (2000) 615.
30. L. Zhang, P. A. Lay, Inorg. Chem. 37 (1998) 1729.
31. T. Li, B. Tian, J. Zhang, R. Dong, T. Wang, F. Yang, Ind. Eng. Chem. Res. 52 (2013) 6704.
32. G. Patwari, B. J. Bodo, R. Singha, P. K. Kalita, Res. J. Chem. Sci. 3, 45 (2013).
33. S.-H. Yang, Y.-J. Lin, H.-C. Chang, Y.-H. Chen, Thin Solid Films 545 (2013) 476.
34. K. Kanamoto, K. Imamura, N. Kataoka, J. Oshitani, H. Imanaka, K. Nakanishi, Colloids Surf. A: Physicochem, Eng. Aspects 350 (2009) 79.
35. S.-Y. Cho, I.-T. Kim, D.-Y. Kim, S. J. Park, B.-K. Kim, J.-H. Lee, Mater. Lett. 32 (1997) 271.
36. Eun-Suk Jeong, In-Hui Hwang, Sang-Wook Han, Langmuir 36 (2020) 10565.
37. Sang-Wook Han, Fundamentals of XAFS, Baleon, (2016).
38. S.-Y. Seo, E.-S. Jeong, C.-H. Kwak, C.-I. Park, Zhelan Jin, S.-H. Kim, S.-W. Han, J. Phys.: Conden. Matter. 25 (2013) 256005.
39. Y. Nagai, T. Hirabayashi, K. Dohmae, N. Takagi, T. Minami, H. Shinjoh, S. Matsumoto, J. Catal. 242, 103 (2006).
40. D. C. Koningsberger, M. K. Oudenhuijen, J. H. Bitter, D. E. Ramaker, Top. Catal. 10 (2000) 167.
41. Dale E. Sayers, Edward A. Stern, Farrel W. Lytle, Phys. Rev. Lett. 27 (1971) 1204.
42. J. J. Rehr, R. C. Albers, Rev. Mod. Phys. 72 (2000) 621.
43. S.-W. Han, Int. J. Nanotechnology 3 (2006) 396.
44. B. Ravel, M. Newville, J. Synchrotron Rad.12 (2005) 537.
45. M. Newville, J. Synchrotron Rad. 8 (2001) 322.
46. S.-W. Han, E. A. Stern, D. Hankel, A. R. Moodenbaugh, Phys. Rev. B. 66 (2002) 94101.
47. V. Luca, S. Djajanti, R. F. Howe, J. Phys. Chem. B 102 (1998) 10650.

48. W. J. H. Borghols, D. Lutzenkirchen-Hecht, U. Haake, W. Chan, U. Lafont, E. M. Kelder, E. R. H. van Eck, A. P. M. Kentgens, F. M. Mulder, M. Wagemaker, J. Electrochem. Soc. 157 (2010) A582.
49. A. L. Ankudinov, B. Ravel, J. J. Rehr, S. D. Conradson, Phys. Rev. B 58 (1998) 7565.
50. J.-S. Jeon, B.-H. Kim, C.-I. Park, S.-Y. Seo, C. H. Kwak, S.-H. Kim, S.-W. Han, Japn. J. Appl. Phys. 49 (2010) 031105.
51. E.-S. Jeong, H.-J. Yu, Y.-J. Kim, Gyu-Chul Yi, Yong-Dae Choi, S.-W. Han, J. Nanosci. Nanotechnol. 10 (2010) 3562.
52. M. D. Segall, P. J. D. Lindan, M. J. Probert, C. J. Pickard, P. J. Hasnip, S. J. Clark, M. C. Payne, J. Phys.: Condens. Matter. 14 (2002) 2717.
53. A. S. Barnard, P. Zapol, J. Phys. Chem. B 108 (2004) 18433.
54. N. Martsinovich, A. Troisi, Phys. Chem. Chem. Phys. 14 (2012) 13392.
55. M. Harb, G. Jeantelot, J.-M. Basset, J. Phys. Chem. C 123 (2019) 28210.
56. Y. Zhou, C. L. Muhich, B. T. Neltner, A. W. Weimer, C. B. Musgrave, J. Phys. Chem. C 116 (2012) 12114.
57. Y. Han, C.-j. Liu, Q. Ge, J. Phys. Chem. B 110 (2006) 7463.
58. Y. Wang, Y. Su, M. Zhu, L. Kang, RSC Adv. 5 (2015) 16582.
59. R. P. Galhenage, H. Yan, S. A. Tenney, N. Park, G. Henkelman, P. Albrecht, D. R. Mullins, D. A. Chen, J. Phys. Chem. C 117 (2013) 7191.
60. J. P. Perdew, K. Burke, M. Ernzerhof, Phys. Rev. Lett. 77 (1996) 3865.
61. S. J. Tauster, S. C. Fung, R. T. K. Baker, J. A. Horsley, Science 211 (1981) 1121.
62. S. J. Tauster , S. C. Fung , R. L. Garten , J. Am. Chem. Soc. 100 (1978) 170.
63. M. S. Spencer, J. Catal. 93 (1985) 216.
64. A. Beck, X. Huang, L. Artiglia, M. Zabilskiy, X. Wang, P. Rzepka, D. Palagin, M.-G. Willinger, J. A. van Bokhoven, Nat. Commun. 11 (2020) 3220.
65. Mi-Young Kim, Jae-Soon Choi, Todd J. Toops, Eun-Suk Jeong, Sang-Wook Han, Viviane Schwartz, Jihua Chen Catalysts 3 (2013) 88.
66. K. Imamura, Y. Tada, H. Tanaka, T. Sakiyama, K. Nakanishi, J. Collid. Inter. Sci. 250 (2002) 409.
67. S.-W. Han, H.-J. Yoo, Sung Jin An, Jinkyoung Yoo, Gyu-Chul Yi, Appl. Phys. Lett. 86 (2005) 21917.
68. Michael Auinger, Vera G. Praig, Bernhard Linder, Herbert Danninger. Corrosion Sci. 96 (2015) 133.
69. M. P. Phaniraj, Dong-Ik Kim, Young Whan Cho, Corrosion Sci. 53 (2011) 4124.

Tables

Table 1: Fit results of EXAFS data of Pt/Ti-FS at the Pt L_3 edge. Data are shown in Fig. 4 (a). *N* is the coordination number, *d* is the distance, and σ^2 is the Debye-Waller factor of atomic pairs. S_0^2 = 0.86 was determined by fitting the EXAFS data of a Pt foil and used in the other fittings.

T (°C)	Pt-O			Pt-Pt(1)			Pt-Pt(2)		
	N	*d* (Å)	σ^2 (Å^2)	*N*	*d* (Å)	σ^2 (Å^2)	*N*	*d* (Å)	σ^2 (Å^2)
RT (Pt-foil)				12.0(7)	2.776(3)	0.005(1)			
RT	5.0(6)	2.021(6)	0.003(1)	5(1)	2.856(9)	0.009(1)	5(1)	3.10(1)	0.010(1)
100	3.6(6)	2.036(7)	0.005(1)	4(1)	2.84(1)	0.013(1)	4(1)	3.08(1)	0.013(1)
150	1.8(6)	2.001(9)	0.005(1)	6(1)	2.73(1)	0.016(1)	2(1)	3.07(2)	0.022(5)
200	1.0(6)	1.94(1)	0.003(2)	8.4(8)	2.682(9)	0.016(1)			
250				8.6(8)	2.686(9)	0.015(1)			
300				8.4(8)	2.673(9)	0.014(1)			
350				8.4(8)	2.680(6)	0.014(1)			
400				8.2(9)	2.685(6)	0.014(1)			
450				9.0(9)	2.661(8)	0.015(1)			
500				9.6(9)	2.673(9)	0.018(2)			
RT^c				9.6(8)	2.682(7)	0.013(1)			

RT^c is the room temperature after being heated up to 500°C and cooled down.

Table 2: Fit results of EXAFS data of H_2O_2-Pt/Ti-FS at the Pt L_3 edge. Data are shown in Fig. 4 (b).

T (°C)	Pt-O			Pt-Pt(1)			Pt-Pt(2)		
	N	*d* (Å)	σ^2 (Å^2)	*N*	*d* (Å)	σ^2 (Å^2)	*N*	*d* (Å)	σ^2 (Å^2)
RT	5.7(7)	2.003(7)	0.003(1)				8(1)	3.28(1)	0.018(2)
100	5.7(7)	2.010(7)	0.004(1)				8(1)	3.22(4)	0.026(5)
150	3.8(7)	2.016(7)	0.004(1)	2(1)	2.75(1)	0.014(1)	6(1)	3.05(1)	0.024(2)
200	1(1)	2.05(1)	0.006(1)	8(1)	2.719(7)	0.014(1)			
250				7.9(8)	2.713(6)	0.012(1)			
300				7.6(8)	2.702(7)	0.012(1)			
350				7.2(8)	2.699(7)	0.011(1)			
400				6.8(8)	2.702(8)	0.011(1)			
450				7.2(8)	2.708(8)	0.013(1)			
500				7.8(9)	2.702(7)	0.014(1)			
RT[c]				7.6(9)	2.730(8)	0.008(1)			

Table 3: Fit results of EXAFS data of anatase TiO_2 powder, Ti-FS, H_2O_2-Ti-FS, Pt/Ti-FS, and H_2O_2-Pt/Ti-FS at the Ti K edge. Data are shown in Fig. 4 (c). S_0^2 = 0.83 was determined by fitting the EXAFS data of the anatase TiO_2 powder and used in the other fittings.

Specimen	T (°C)	Ti-O(1)			Ti-O(2)			Ti-Ti(1)			Ti-Ti(2)		
		N	*d* (Å)	σ^2 (Å^2)	*N*	*d* (Å)	σ^2 (Å^2)	*N*	*d* (Å)	σ^2 (Å^2)	*N*	*d* (Å)	σ^2 (Å^2)
Anatase TiO_2	RT	2.2(3)	1.859(5)	0.003(1)	4.3(5)	1.964(5)	0.003(1)	4.0(3)	3.044(5)	0.006(1)	4.0(3)	3.791(5)	0.006(1)
Ti-FS	RT	3.7(7)	1.946(8)	0.010(1)				2(1)	3.01(1)	0.013(1)			
	500	3.2(7)	1.884(8)	0.007(1)				2(1)	2.96(2)	0.019(4)			
	RT[c]	3.2(7)	1.903(8)	0.005(1)				2(1)	3.01(1)	0.014(2)			
H_2O_2-Ti-FS	RT	1.6(7)	2.17(1)	0.005(1)	3.2(7)	1.988(8)	0.005(1)	2.8(7)	3.33(1)	0.008(1)			
Pt/Ti-FS	RT	1.6(4)	1.816(5)	0.003(1)	3.2(8)	1.993(5)	0.003(1)	3(1)	3.00(1)	0.012(1)	3(1)	3.94(1)	0.009(1)
	250	1.6(4)	1.815(4)	0.003(1)	3.6(8)	1.994(7)	0.003(1)	3(1)	3.00(1)	0.010(1)	3(1)	3.76(4)	0.020(7)
H_2O_2-Pt/Ti-FS	RT	1.6(4)	1.973(5)	0.010(1)	3.2(8)	1.982(5)	0.010(1)	3(1)	2.99(2)	0.014(2)	4(1)	3.94(2)	0.017(4)
	250	1.6(4)	1.943(5)	0.012(1)	3.6(8)	1.952(8)	0.012(1)	3(1)	2.90(1)	0.010(1)	4(1)	3.71(1)	0.009(2)

Figures

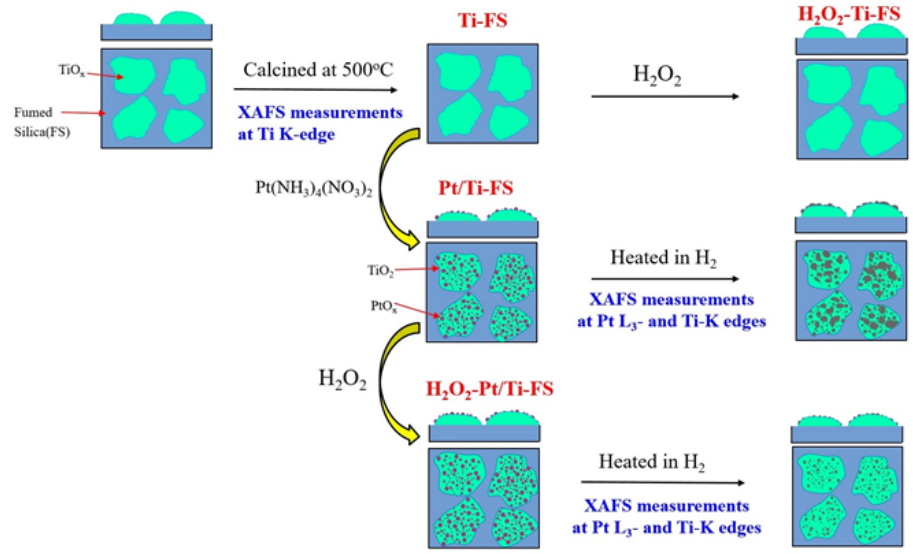

Figure 1

Synthesis procedure of Pt/Ti-FS, specimen names, and conditions of XAFS measurements

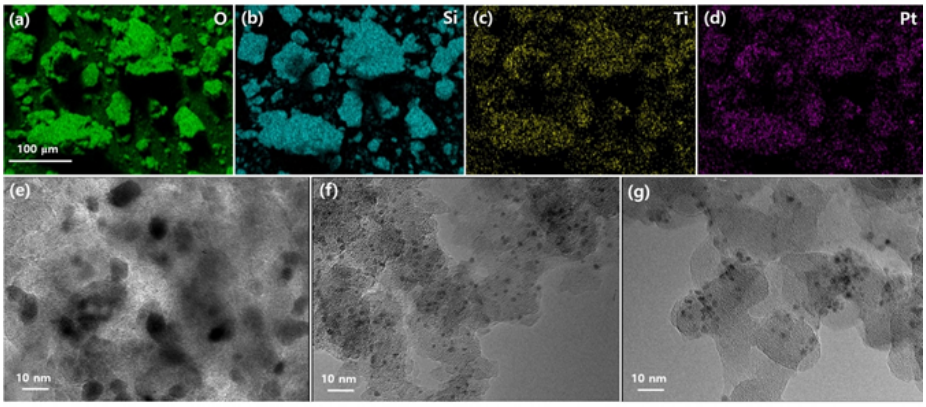

Figure 2

EDS images of H_2O_2-Pt/Ti-FS for (a) O, (b) Si, (c) Ti, and (d) Pt atoms. TEM images of (e) Pt-FS, (f) Pt/Ti-FS, and (g) H_2O_2-Pt/Ti-FS.

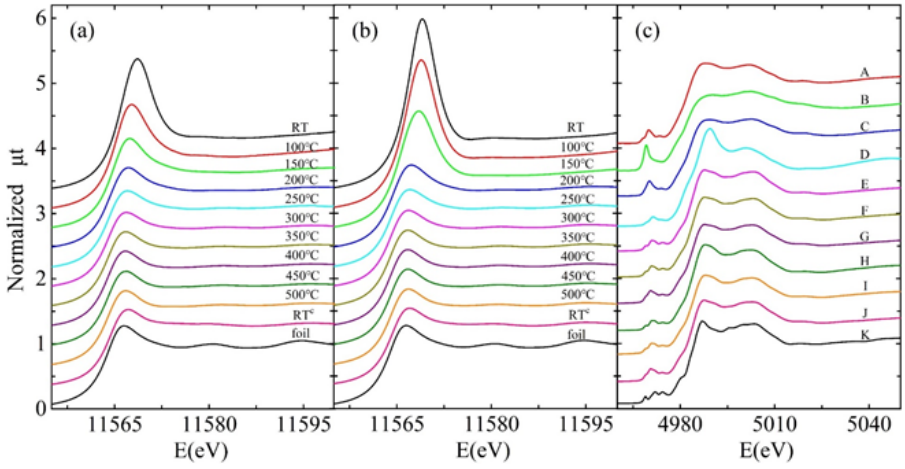

Figure 3

Normalized XANES (μt) spectra of (a) Pt/Ti-FS and (b) H_2O_2-Pt/Ti-FS at the Pt L_3 edge at different temperatures. (c) XANES spectra at the Ti K edge of A Ti-FS at RT, B Ti-FS at 500°C, C Ti-FS at RT^c, D H_2O_2-Ti-FS at RT, E Pt/Ti-FS at RT, F Pt/Ti-FS at 100°C, G Pt/Ti-FS at 250°C, H H_2O_2-Pt/Ti-FS at RT, I H_2O_2-Pt/Ti-FS at 100°C, J H_2O_2-Pt/Ti-FS at 250°C, and K anatase TiO_2 at RT. RT^c indicates RT after being heated up to 500°C and cooled down. XANES measurements were taken under an H_2 environment except for H_2O_2-Ti-FS and anatase TiO_2, which were taken in air.

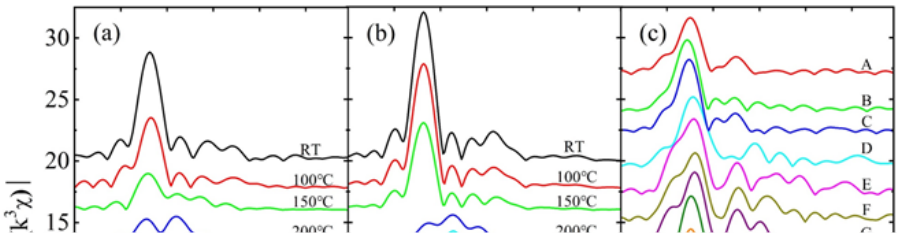

Figure 4

Magnitude of FT-EXAFS ($|k^3\chi)|$ as functions of the distance from a Pt atom of (a) Pt/Ti-FS and (b) H_2O_2-Pt/Ti-FS at different temperatures. (c) EXAFSs as functions of the distance from a Ti atom of A Ti-FS at RT, B Ti-FS at 500°C, C Ti-FS at RT^c, D H_2O_2-Ti-FS at RT, E Pt/Ti-FS at RT, F Pt/Ti-FS at 100°C, G Pt/Ti-FS at 250°C, H H_2O_2-Pt/Ti-FS at RT, I H_2O_2-Pt/Ti-FS at 100°C, J H_2O_2-Pt/Ti-FS at 250°C, and K anatase TiO_2 at RT. For the Fourier transform, the EXAFS data in the k-range from 2.5 – 10.5 $Å^{-1}$ and a Hanning window with a windowsill with of 0.5 $Å^{-1}$ were used.

Figure 5

Representative FT-EXAFS data and the best fits. At the Pt L_3 edge of A Pt/Ti-FS and B H_2O_2-Pt/Ti-FS at different temperatures of (a) RT, (b) 200°C, and (c) RT^c, respectively. (d) At the Ti Kedge of Pt/Ti-FS and H_2O_2-Pt/Ti-FS at 250°C. Data in the r-ranges from 1.3 – 3.5 Å and from 1.3 – 4.3 Å were respectively fitted for the Pt L_3 and Ti K edges.

Figure 6

(a) and (b) Top and side views of anatase TiO_2(101) surface, respectively. Top views of (c_1) bare-TiO_2(101), (d_1) oxidized-TiO_2(101), and (e_1) reduced-TiO_2(101) surfaces, respectively. The green vertical arrows in (d_1) and (e_1) indicate added and removed O atoms, respectively. DFT calculation results with a Pt adatom on (c_2) bare-TiO_2(101), (d_2) oxidized-TiO_2(101), and (e_2) reduced-TiO_2(101) surfaces, respectively. ΔE is the total energy change due to a Pt adatom, and it is described in the text. (c_3), (d_3), and (e_3) are the side views of (c_2), (d_2), and (e_2), respectively. The gray, red, and blue symbols are Ti, O, and Pt atoms, respectively.

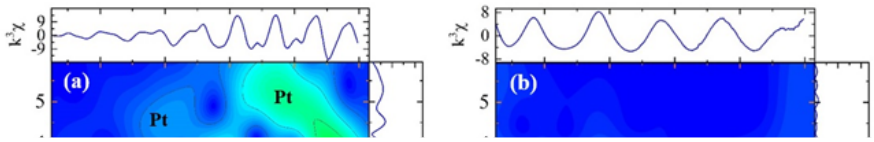

Figure 7

At Pt L_3 edge, WT-EXAFS of (a) Pt foil at RT, (b) RT, (c) 200^{o}C, and (d) RT^{c} of H_2O_2-Pt/Ti-FS. The top and the right data are the measured EXAFS in the k-space and FT-EXAFS in the r-space, respectively.